Sudestada1, a Drosophila ribosomal prolyl-hydroxylase required for mRNA translation, cell homeostasis, and organ growth

Maximiliano J. Katz, Julieta M. Acevedo, Christoph Loenarz, Diego Galagovsky, Phebee Liu-Yi, Marcelo Pérez-Pepe, Armin Thalhammer, Rok Sekirnik, Wei Ge, Mariana Melani, et al.

Sudestada1, a *Drosophila* ribosomal prolyl-hydroxylase required for mRNA translation, cell homeostasis, and organ growth

Maximiliano J. Katz[a,b,1], Julieta M. Acevedo[a,b,1], Christoph Loenarz[c], Diego Galagovsky[a,b], Phebee Liu-Yi[d], Marcelo Pérez-Pepe[a,b], Armin Thalhammer[c], Rok Sekirnik[c], Wei Ge[c], Mariana Melani[a,b], María G. Thomas[a,b], Sergio Simonetta[a,b], Graciela L. Boccaccio[a,b,e], Christopher J. Schofield[c], Matthew E. Cockman[d], Peter J. Ratcliffe[d], and Pablo Wappner[a,b,e,2]

[a]Fundación Instituto Leloir, C1405BWE Buenos Aires, Argentina; [b]Consejo Nacional de Investigaciones Científicas y Técnicas, C1405BWE Buenos Aires, Argentina; [c]Chemistry Research Laboratory and Oxford Centre for Integrative Systems Biology, University of Oxford, Oxford OX1 3TA, United Kingdom; [d]Centre for Cellular and Molecular Physiology, University of Oxford, Oxford OX3 7BN, United Kingdom; and [e]Departamento de Fisiología, Biología Molecular y Celular, Facultad de Ciencias Exactas y Naturales, Universidad de Buenos Aires, 1428 Buenos Aires, Argentina

Edited by William G. Kaelin, Jr., Harvard Medical School, Boston, MA, and approved December 23, 2013 (received for review July 31, 2013)

Genome sequences predict the presence of many 2-oxoglutarate (2OG)-dependent oxygenases of unknown biochemical and biological functions in *Drosophila*. Ribosomal protein hydroxylation is emerging as an important 2OG oxygenase catalyzed pathway, but its biological functions are unclear. We report investigations on the function of Sudestada1 (Sud1), a *Drosophila* ribosomal oxygenase. As with its human and yeast homologs, OGFOD1 and Tpa1p, respectively, we identified Sud1 to catalyze prolyl-hydroxylation of the small ribosomal subunit protein RPS23. Like OGFOD1, Sud1 catalyzes a single prolyl-hydroxylation of RPS23 in contrast to yeast Tpa1p, where Pro-64 dihydroxylation is observed. RNAi-mediated Sud1 knockdown hinders normal growth in different *Drosophila* tissues. Growth impairment originates from both reduction of cell size and diminution of the number of cells and correlates with impaired translation efficiency and activation of the unfolded protein response in the endoplasmic reticulum. This is accompanied by phosphorylation of eIF2α and concomitant formation of stress granules, as well as promotion of autophagy and apoptosis. These observations, together with those on enzyme homologs described in the companion articles, reveal conserved biochemical and biological roles for a widely distributed ribosomal oxygenase.

fruit fly | ribosome | dioxygenase | proline | tranlational stress

Iron [Fe(II)]- and 2-oxoglutarate (2OG)-dependent oxygenases are a superfamily with diverse biochemical and biological functions. During 2OG oxygenase catalysis, substrate oxidation is coupled to decarboxylation of 2OG, yielding succinate and carbon dioxide (1, 2). Structural studies reveal that the catalytic domain of 2OG oxygenases contains a conserved double-stranded β-helix (DSBH) fold presenting an HXD. . .H facial triad motif that coordinates an Fe(II) cofactor (3, 4). These and other structural features have been used to predict the existence of multiple uncharacterized 2OG oxygenases. In contrast to microorganisms and plants where 2OG oxygenases catalyze a wide variety of oxidative reactions, in animals their biochemical activities appear limited to hydroxylations or demethylations via hydroxylation (1, 5, 6). Despite progress in making biochemical assignments, the physiological roles of most 2OG oxygenases predicted by bioinformatic analysis of animal genomes are unknown. For instance, we have identified ∼50 putative 2OG oxygenases in the *Drosophila* genome, but only a few are characterized (7, 8).

The function of Fatiga, the single *Drosophila* homolog of human hypoxia inducible transcription factor (HIF) prolyl-4-hydroxylases (PHDs), has been well studied in the context of oxygen sensing (9). HIF prolyl-hydroxylation plays a central role in the animal hypoxic response via hydroxylation of HIF, a posttranslational modification that signals for HIF-α degradation in a physiologically relevant oxygen-dependent manner (10, 11). Given the tractability of these enzymes as targets for pharmacological modulation by 2OG analogs and related compounds, elucidation of the function of related 2OG oxygenases in biology is an area of current interest (12, 13).

To identify other oxygenase-catalyzed reactions with signaling roles, we have conducted an RNAi-based screen of 2OG oxygenases for phenotypes in *Drosophila*. We identified CG44254, a highly conserved gene that is distantly related to oxygen sensing PHDs (14), as necessary for normal growth and mRNA translation in the fly. This gene, which we have termed *sudestada1* (*sud1*) after a wind that blows across the southeastern coast of South America, is highly conserved from yeast to humans; homologous genes in *Saccharomyces cerevisiae* (*TPA1*) (15, 16), *Schizosaccharomyces pombe* (*Ofd1*) (17, 18), and *Homo sapiens* (*OGFOD1*) (19, 20) have been implicated in translation termination, oxygen-dependent regulation of the transcription factor Sre1N, and translational stresses responses, respectively.

In independent work, reported in companion articles, we discovered that Tpa1p, Ofd1, and OGFOD1 are protein hydroxylases

Significance

Emerging evidence indicates that posttranslational hydroxylation of intracellularly localized proteins is more prevalent than once thought. We identify *Drosophila melanogaster sudestada1 (sud1)* as a gene that is needed for normal growth in the fly and show that *sud1* encodes a prolyl-hydroxylase that catalyzes posttranslational hydroxylation of a conserved residue in the small ribosomal subunit protein RPS23. Knockdown of Sud1 results in growth impairment and reduced RPS23 hydroxylation, which is associated with activation of the unfolded protein response, induction of apoptosis, and increased autophagy. Together with findings in humans and yeast reported in the companion articles, the work reveals a new type of posttranslational ribosome modification that is highly conserved in eukaryotes.

Author contributions: M.J.K., J.M.A., C.L., D.G., R.S., W.G., M.M., M.G.T., S.S., G.L.B., C.J.S., M.E.C., P.J.R., and P.W. designed research; M.J.K., J.M.A., C.L., D.G., P.L.-Y., R.S., W.G., M.M., S.S., and M.E.C. performed research; A.T. contributed new reagents/analytic tools; M.J.K., J.M.A., C.L., D.G., P.L.-Y., M.P.-P., R.S., W.G., M.M., M.G.T., S.S., G.L.B., C.J.S., M.E.C., P.J.R., and P.W. analyzed data; and M.J.K., J.M.A., C.L., M.M., G.L.B., C.J.S., M.E.C., P.J.R., and P.W. wrote the paper.

The authors declare no conflict of interest.

This article is a PNAS Direct Submission.

Freely available online through the PNAS open access option.

[1]M.J.K. and J.M.A. contributed equally to the work.

[2]To whom correspondence should be addressed. E-mail: pwappner@leloir.org.ar.

This article contains supporting information online at www.pnas.org/lookup/suppl/doi:10.1073/pnas.1314485111/-/DCSupplemental.

that catalyze unique di- and monohydroxylations of a conserved prolyl residue in the small ribosomal subunit protein RPS23 (21, 22). Here we describe the biochemical and physiological characterization of Sud1 in *Drosophila melanogaster*. We show that Sud1 is a dioxygenase that catalyses monohydroxylation of RPS23 in the fly and that its silencing results in growth defects and impairment of mRNA translation, along with the induction of Eukaryotic Initiation Factor 2α (eIF2α) phosphorylation, stress granule formation, autophagy and apoptosis.

Results

Sudestada1 Encodes the *Drosophila* Tpa1p/OGFOD1 Homolog and Is Required for Normal Growth. In initial studies, we carried out an RNAi screen in *Drosophila* to identify 2OG oxygenases that lead to impaired growth after knockdown (Table S1). These studies led to the identification of a potential *Ofd1/TPA1/OGFOD1* homolog (*CG44254*) that we name *sudestada1* (*sud1*). Two transcripts generated by alternative splicing, *sud1* and *sud2,* are reported in databases that curate high-throughput transcriptomic data (http://flybase.org) (Fig. S1*A*). RT-PCR analyses confirm the expression of both transcripts in larvae (Fig. S1 *B* and *C*). Only Sud1 includes a predicted oxygenase domain encompassing residues 171–275 that manifests a substantial degree of identity with Tpa1p/Ofd1/OGFOD1 (Fig. S1 *D* and *E*). Sud2 encodes a predicted phosphatidylinositol-glycan biosynthesis class S protein that is apparently unrelated to oxygenases and has not been investigated in this work.

We then analyzed the mRNA expression profile of *sud1* through the fly life cycle. Quantitative real-time RT-PCR (qRT-PCR) assays reveal *sud1* mRNA expression at all developmental stages, with the highest levels at the first larval instar (Fig. 1*A*). We then compared expression in third-instar larval tissues and found that *sud1* mRNA is highly expressed in the fat body, with significant expression in other organs including the brain, salivary glands, imaginal discs, and gut (Fig. 1*B*). To study the subcellular localization of Sud1, we generated a Sud1-GFP fusion construct and expressed this using the Gal4-UAS system in different tissues (Fig. 1 *C–H*); Sud1 localizes predominantly to the nucleus, although lower levels are also detected in the cytoplasm.

To investigate Sud1 functions, we first expressed a double-stranded RNA that specifically targets *sud1* sequences, without affecting *sud2* mRNA levels (Fig. S1 *B* and *C*). Given that *S. cerevisiae* Tpa1p and *S. pombe* Ofd1 have putative active sites in the *N*-terminal of their two DSBH domains that possess similarity to PHD2 (15, 23), we tested whether Sud1 plays a role in the HIF-dependent transcriptional response to hypoxia by observing the effects of Sud1 knockdown on HIF/Sima-dependent transcription in the embryonic tracheal system. Embryos expressing *sud1* RNAi failed to modulate a HIF-dependent transcriptional reporter, whereas, as expected, embryos that express an RNAi targeting the prolyl-4-hydroxylase gene *fatiga* displayed strong up-regulation of the same reporter under mild hypoxic conditions, providing a positive control for the assay (Fig. S2 *A–D*).

Ubiquitous *sud1* RNAi expression mediated by an *actin*-Gal4 driver was lethal at the second larval instar. To enable phenotypic analysis of the effect of Sud1 suppression at later developmental stages, we used more restricted RNAi interventions. Because Sud1 is most expressed in the fat body, we expressed *sud1* RNAi in this organ, using the driver *pumpless*-Gal4 (*ppl*-Gal4). Restricted silencing allowed development of viable adults. Analysis of the fat body of third-instar larvae of such flies revealed a significant reduction of cell size (Fig. 2 *A–C*). Because reduction of fat body size can have a systemic effect on body growth (24, 25), we measured pupal size and observed a significant reduction in the volume of individuals expressing *sud1* RNAi in the fat body (Fig. 2 *D* and *E*). To determine whether Sud1 suppression impairs growth in other fly organs, *sud1* RNAi was expressed in the wing imaginal disc. In both the posterior (Fig. 2 *F–H*) and the dorsal (Fig. S2 *E* and *F*) compartments of the disc, *sud1* RNAi significantly reduced growth. To verify that the effect of the RNAi is due to Sud1 silencing, the homologous *Drosophila willistoni sud1* gene was coexpressed and found to restore the growth defect (Fig. 2*H*). To test whether Sud1 function is conserved across species, we coexpressed human *OGFOD1*, together with *sud1* RNAi, in the wing posterior compartment. Although incomplete, we again observed restoration of the growth that had been reduced by Sud1 silencing (Fig. 2*H*), implying that the mammalian and fly dioxygenases are functionally conserved.

We next studied effects on cell size. Because all epidermal cells of the *Drosophila* wing produce a single cuticular hair, hair density was used to assess cell density and hence to calculate both cell size and cell number in the wing posterior compartment. In comparison with control RNAi, *engrailed*-Gal4–driven expression of *sud1* RNAi induced an increase in cell density (Fig. 2 *I–K*), indicating that the 21% reduction of the wing posterior compartment (Fig. 2*K*) arose from both a reduction in cell size (15%) and a reduction in cell number (6%).

Sudestada1 Hydroxylates the Ribosomal Protein RPS23. It is known that mutations in ribosomal proteins can provoke growth defects in *Drosophila*, such as those observed after Sud1 knockdown (26, 27). Consistent with this, in refs. 21 and 22, it is shown that the Sud1 homologs in humans and yeast catalyze a posttranslational modification of a protein of the small ribosomal subunit termed RPS23. Whereas human OGFOD1 mediates monohydroxylation of proline 62 of RPS23, yeast Tpa1p/Ofd1 and its green algae homolog catalyze dihydroxylation of the analogous prolyl residue.

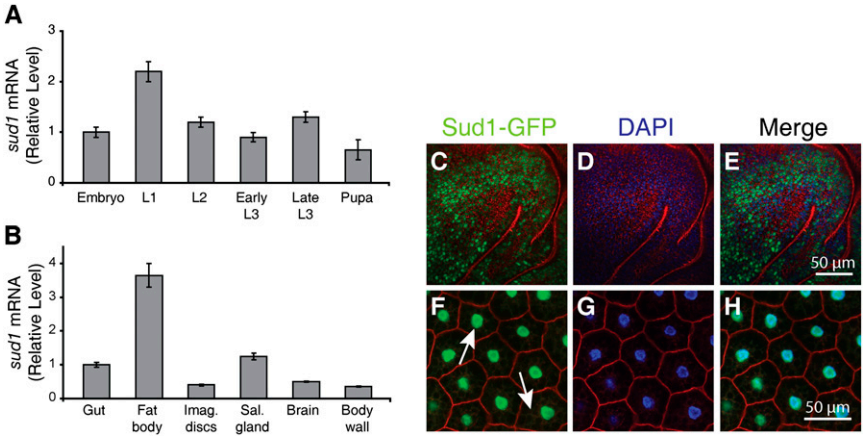

Fig. 1. Expression and subcellular localization of *sudestada*1. (*A*) Temporal *sud1* expression pattern throughout the fly life cycle, as determined by real-time RT-PCR (qRT-PCR); error bars represent SD. (*B*) Expression of *sud1* mRNA in different organs of third-instar larvae. (*C–H*) Expression of a UAS-Sud1-GFP fusion construct in wing imaginal discs (*C–E*) or the fat body (*F–H*). In both tissues, the protein is mostly nuclear, although some GFP signal can be seen at the cytoplasm (arrows in *F*).

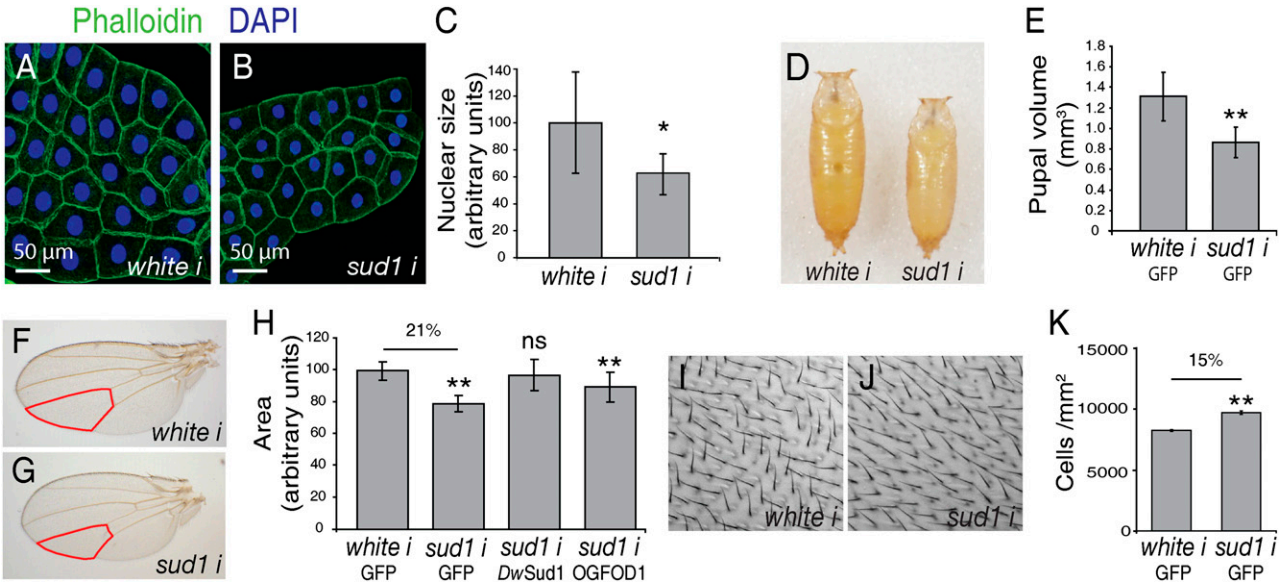

Fig. 2. Sud1 loss of function affects growth. (*A–C*) Sud1 silencing in the fat body of third-instar larvae provokes cell size reduction. *white* (control) (*A*) or *sud1* (*B*) double-stranded RNAs were expressed under control of a *pumpless*-Gal4 (*ppl*-Gal4) driver; fat body cells expressing *sud1* RNAi are smaller than those of the control as assessed by quantification of the area of cell nuclei (*C*). $n = 3$ independent experiments, error bars represent SD, and $^*P < 0.01$ (Student *t* test). (*D* and *E*) As a consequence of *ppl*-Gal4–driven expression of *sud1* RNAi, pupal volume is reduced in comparison with that of a control line expressing a *white* RNAi. $n \geq 25$ in three independent experiments. Error bars represent SD; $^{**}P < 0.001$ (Student *t* test). (*F–H*) Expression of *sud1* RNAi in the wing disc posterior compartment results in growth impairment: the area limited by wing veins L4, L5, the posterior cross-vein, and the wing margin (marked in red in *F* and *G*) was measured as an indication of the variation of the area of the posterior compartment; (*H*) area quantification after *sud1* RNAi expression, and rescue of the WT wing phenotype after concomitant expression of a *Drosophila willistoni sud1* or human *OGFOD1* transgenes (DwSud1; OGFOD1); the rescue after expression of human OGFOD1 was partial. $n \geq 30$ in three independent experiments. Error bars represent SD ($^{**}P < 0.001$; one-way ANOVA with Tukey post hoc test). (*I–K*) Cell size and cell number are both reduced after expression of *sud1* dsRNA: wing hair density increases after expression of *sud1* RNAi (*K*), indicating that cell size is reduced. Cell size reduction (15%) accounts only partially for reduction of the area of the wing posterior compartment after *sud1* RNAi treatment (21%) (cf. *H* and *K*). The remaining area reduction is due to a decreased number of cells in the compartment (6%). $n \geq 10$ in three independent experiments. Error bars represent SD ($^{**}P < 0.001$; Student *t* test).

Sequence alignments reveal that the RPS23 prolyl residue that is subject to Tpa1p/OGFOD1-dependent hydroxylation is conserved in *Drosophila* (Fig. 3*A*).

We therefore investigated whether *Drosophila* RPS23 is post-translationally modified. Ribosomes were purified from *Drosophila* Schneider2 (S2) cells grown in culture and then subjected to ultra-performance liquid chromatography (UPLC)-coupled intact protein mass spectrometric analysis. A species corresponding to *Drosophila* RPS23 was observed with a mass +16 Da greater than that predicted from the primary sequence, consistent with addition of a single oxygen atom (Fig. 3*B*). To investigate the dependence of this modification on Sud1, S2 cells were treated with *sud1* RNAi, and LC-MS analyses were performed on Arg-C–digested ribosomal RPS23 preparations. Consistent with the whole-protein MS data (Fig. 3*B*), a peptidic fragment containing Pro-62 was observed with a mass increment of +16 Da. No unmodified species was observed in material prepared from untreated cells, consistent with RPS23 being monohydroxylated. However, after Sud1 silencing, a second species corresponding to the unhydroxylated parent peptide became apparent (Fig. 3 *C* and *D* and Fig. S3 *A* and *B*), indicating that Sud1 is necessary for the hydroxylation. To directly investigate whether Sud1 catalyses RPS23 prolyl hydroxylation, we prepared recombinant RPS23 either alone or coexpressed with Sud1 in a His-tagged form in *Escherichia coli*. A tryptic RPS23 fragment (residues 55–67) revealed a mass shift of +16 Da, which was assigned using MS/MS analyses to Pro-62, implying that Sud1 is the RPS23 prolyl monohydroxylase (Fig. 3E and Fig S3 *C–E*). In none of the studies on Sud1/RPS23, either on cellular prepared material or when working with purified protein, did we observe evidence of a +32-Da mass shift corresponding to di-hydroxylation of RPS23 as observed for yeast Tpa1p/Ofd1 and green algae (*Ostreococcus tauri*) otOGFOD1 (21). Taken together, these experiments indicate that Sud1 catalyzes mono-, but not dihydroxylation of RPS23 Pro-62.

Sudestada1 Knockdown Affects Protein Synthesis and Triggers the Unfolded Protein Response. To further investigate the effects of Sud1 knockdown, we analyzed the effects of *sud1* RNAi on protein synthesis. Wing imaginal discs, ubiquitously expressing either *sud1* or a control dsRNA, were incubated with [^{14}C]-labeled amino acids, and incorporation into protein was measured. A significant decrease of protein synthesis occurred in discs expressing *sud1* RNAi in comparison with controls (Fig. S4 *A* and *B*). Next, we analyzed the phosphorylation status of the translation initiation factor eIF2α, a key regulatory step in the control of cap-dependent mRNA translation. Sud1 silencing in the posterior wing disc compartment promotes substantial increase in P-eIF2α staining that is clearly limited to the posterior wing disc compartment, whereas in flies expressing control RNAi, P-eIF2α was evenly distributed across the whole disc (Fig. 4 *A–D*). This effect was specifically dependent on Sud1 silencing, because coexpression of the *Drosophila willistoni sud1* transgene largely suppressed the induction of P-eIF2α (Fig. S4 *C–F*). This effect of *sud1* RNAi on eIF2α phosphorylation was further confirmed by immunoblotting of extracts prepared from cultured S2 cells after treatment with *sud1* RNAi (Fig. 4*E*). Because eIF2α phosphorylation induces stress granule formation (28), we analyzed for Sud1-linked formation of stress granules. Extensive stress granule formation was observed in S2 cells treated with *sud1* RNAi compared with control RNAi (Fig. 4 *F–I* and Fig. S4 *G* and *H*). Together, these experiments suggest that Sud1 knockdown leads to increased eIF2α phosphorylation, which in turn diminishes protein synthesis and promotes stress granule accumulation.

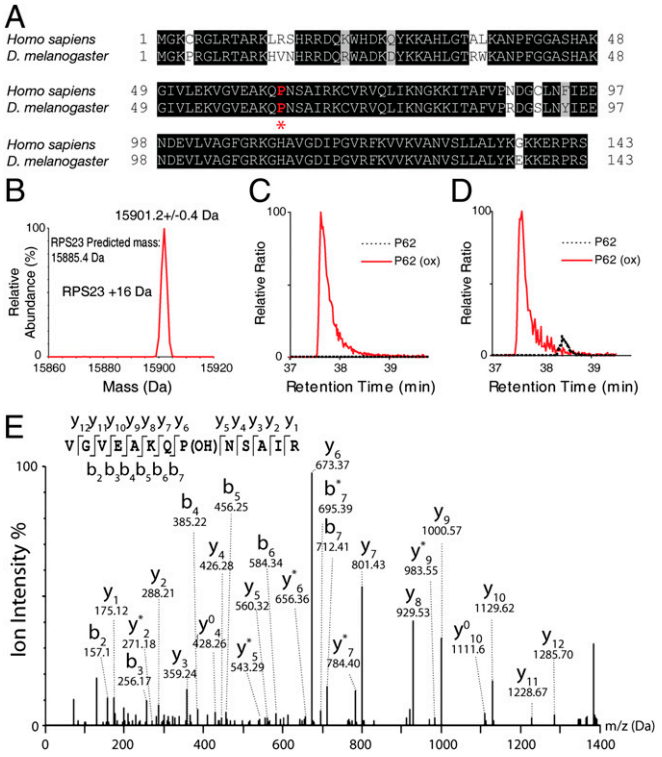

Fig. 3. Sudestada1 hydroxylates RPS23. (*A*) *Drosophila* and human ribosomal protein RPS23 are almost identical. Conserved residues between the two proteins are marked in black; Pro-62 is highlighted in red and marked with an asterisk. (*B*) Deconvoluted ESI-MS whole protein spectrum of *D. melanogaster* RPS23 isolated from S2 cell ribosomes purified by sucrose density sedimentation followed by online UPLC mass spectrometry. A mass of 15,901.2 Da is consistent with a +16-Da shift relative to predicted mass of 15,885.4 Da (*N*-terminal methionine cleaved), indicative of oxidative modification. Note there is no evidence for proline dihydroxylation. (*C* and *D*) Hydroxylation of RPS23 is suppressed by *sud1* dsRNA. Extracted ion chromatograms of *m/z* 670.057 and *m/z* 675.39 corresponding to unhydroxylated (dashed line) and hydroxylated (solid red line) forms of the Pro-62 containing RPS23 peptide GIVLEKVGVEAKQPNSAIR ($[M+3H]^{3+}$) isolated from S2 cells treated with control (*C*) or *sud1* dsRNA (*D*) (see Fig S3 *A* and *B* for assignment of species). (*E*) LC-MS/MS analysis of trypsinized GST-RPS23 after coexpression with Sudestada1. MS/MS spectrum of trypsinized RPS23 after coexpression with His_6-Sudestada1 in *E. coli* reveals a peptide, 55-VGVEAKQPNSAIR-67, with a complete series of y-ions demonstrating monohydroxylation (+16 Da) at Pro-62. The b and y fragment ions are indicated (peptide precursor ion: M_r 1,383.760048 Da; calculated 1,383.7470 Da; see Fig. S3*E* for assignment of species).

Because eIF2α phosphorylation is triggered by the unfolded protein response (UPR) (29), among other stimuli, we investigated whether the UPR is triggered by Sud1 knockdown. As a marker of UPR induction, we measured splicing of *xbp1* mRNA, a transcription factor that induces ER chaperones and that is activated by splicing in response to UPR. We used transgenic flies expressing an Xbp1-GFP reporter that generates an in-frame transcript when splicing of the *xbp1* mRNA has occurred (30). This reporter was coexpressed in the wing disc posterior compartment, along with *sud1* RNAi or a control RNAi. As expected, *xbp1* splicing did not occur with expression of the control RNAi (Fig. 4 *J–J″*), but was strongly induced both by exposure of the discs to DTT (DTT is an established inducer of UPR; Fig. 4 *K–K″*) and by expression of *sud1* RNAi (Fig. 4 *L–L″*). Consistent with activation of *xbp1* splicing, ubiquitous expression of *sud1* RNAi at the first larval instar provoked the up-regulation of the endogenous Xbp1 target gene *bip1*, as determined by RT-PCR (Fig. S4*I*). To investigate the extent to which UPR activation and eIF2α phosphorylation account for Sud1-dependent growth impairment, we studied growth of the wing posterior compartment in flies coexpressing the *sud1* RNAi simultaneously with an RNAi targeting *perk*, the *Drosophila* ortholog of PKR-related ER kinase (PERK). Silencing of PERK partially suppresses the reduction of growth induced by Sud1 knockdown (Fig. 4 *M* and *N*), suggesting that UPR activation accounts, at least in part, for the observed growth impairment.

Sudestada1 Knockdown Triggers Autophagy and Apoptosis. One consequence of UPR activation is induction of autophagy (31). Autophagy affects growth by reducing cell size in various *Drosophila* tissues (32), so we hypothesized that autophagy contributes to the growth impairment observed with Sud1 silencing. Consistent with this, *sud1* RNAi expression in the wing disc posterior compartment provoked induction of autophagy markers in this disc territory, including nucleation of the ATG8-GFP autophagy marker (Fig. 5 *A* and *B*); accumulation of the fluorescent lysosomal probe lysotracker (Fig. 5 *C* and *D*); and formation of large Lamp1-GFP foci (Fig. 5 *E* and *F*). Expression of the *D. willistoni sud1* transgene abolished lysosomal dye accumulation at the posterior disc compartment, again indicating that the action of *sud1* silencing on autophagy is target specific (Fig. S5 *A–C*).

Finally, we investigated whether the reduction in the number of cells observed following expression of *sud1* RNAi (Fig. 2 *I* and *J*) is due to reduced cell proliferation or increased cell death. Phospho-histone3 staining analysis revealed that expression of *sud1* dsRNA in the wing disc posterior compartment does not decrease cell proliferation (Fig. S5*D*), whereas TUNEL staining assays revealed that apoptosis was triggered by *sud1* RNAi (Fig. 5 *G–J*). Reduction of the area of the posterior compartment of the wing following Sud1 silencing was partially suppressed by concomitant expression of the caspase inhibitor p35 (Fig. S5*E*), confirming that induction of apoptosis accounts in part for growth impairment.

Given that the Target of Rapamicin (TOR) pathway plays a central role in growth regulation in the fat body (32), we analyzed genetic interactions between Sud1 and genes of this pathway in this organ. Interestingly, reduction of function of the TOR pathway led to partial suppression of growth defects provoked by Sud1 silencing (Table S2). These results suggest that slowing down translation, as a consequence of TOR down-regulation (33), alleviates the translational stress provoked by Sud1 knockdown.

Discussion

Ribosomal protein hydroxylation mediated by 2OG oxygenases is emerging as an important evolutionary conserved pathway (34). We analyzed the function of Sudestada1, a *Drosophila* oxygenase homolog of human OGFOD1, *S. cerevisiae* Tpa1p, and *S. pombe* Ofd1. We demonstrated that, like OGFOD1, Sud1 mediates hydroxylation of proline 62 of the small ribosomal subunit protein RPS23. Importantly, Sud1 catalyzes a single prolyl hydroxylation, as observed for human OGFOD1 but contrasting with homologs from lower eukaryotes including Tpa1p in yeast, where RPS23 is di-hydroxylated (21). Thus, RPS23 Pro-62 hydroxylation is a unique and highly conserved ribosomal posttranslational modification, but there appears to be a clear biochemical difference between the extent (i.e., mono- or di-) of RPS23 hydroxylation in animals and lower eukaryotes.

Reduction of Sud1 levels causes growth impairment in various *Drosophila* tissues, as observed for OGFOD1 in some human-derived cells (22). The growth defects associated with Sud1 silencing correlated with translational stress, characterized by phosphorylation of eIF2α, the formation of stress granules, induction of UPR, and promotion of autophagy and apoptosis. These findings, along with those on the human and yeast homologs described in the accompanying manuscripts (21, 22), reveal a biochemically

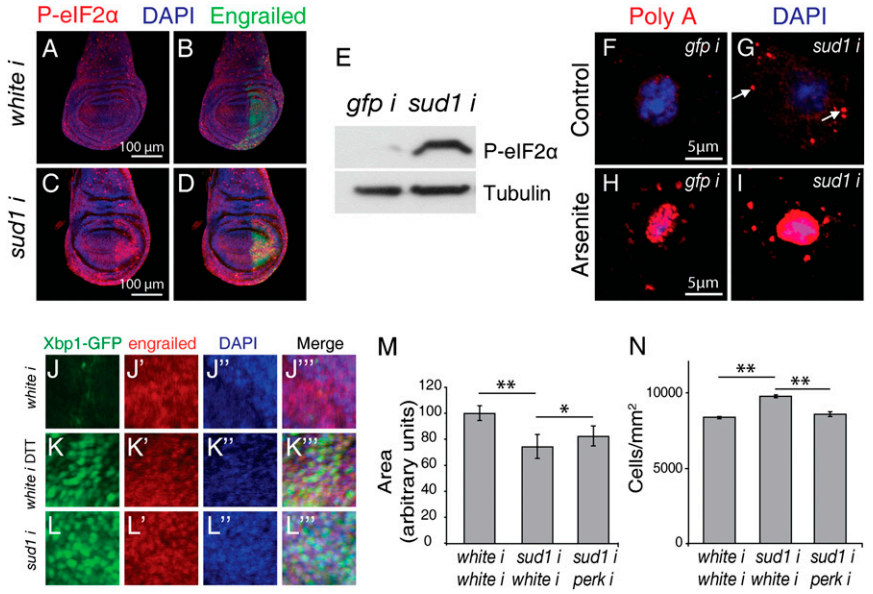

Fig. 4. Sudestada1 knockdown affects protein synthesis and leads to activation of the unfolded protein response. (*A–D*) Phosphorylation of eIF2α is induced at the wing disc posterior compartment after expression of a *sud1* RNAi (*C* and *D*) but not of a *white* RNAi (*A* and *B*), as revealed by anti–P-eIF2α immunofluorescence (red); anti-Engrailed–positive staining identifies the disc posterior compartment (green) (*B* and *D*); DAPI labels cell nuclei (blue). (*E*) Anti–phospho-eIF2α western blot analysis of S2 cell extracts shows that *sud1* but not *gfp* (control) RNAi treatment promotes eIF2α phosphorylation. (*F–I*) Sud1 silencing induces stress granules (SGs) formation. S2 cells treated with a *sud1* RNAi (*G* and *I*) exhibit more stress granules than cells treated with a control *gfp* RNAi (arrow, *F* and *H*), as revealed by polyA FISH. SGs increase after *sud1* silencing occurs both in untreated cells (*F* and *G*) and in cells exposed to sodium arsenite for 2 h (*H* and *I*). (J–L′′′) *xpb1*splicing is activated after *sud1* knockdown. An Xbp1-GFP splicing reporter was expressed at the disc posterior compartment through an *en*-Gal4 driver, and expression was detected with an anti-GFP antibody; a portion of the disc posterior compartment is shown in J–L′′′. The reporter is silent in discs expressing a *white* (control) dsRNA (*J*) and is activated after DTT treatment (*K*) or expression of *sud1* RNAi (*L*). In *J′*, *K′*, and *L′*, anti-Engrailed immunostaining confirms the expression of this posterior compartment-specific marker. Wing posterior compartment area (*M*) and cell size (*N*) reduction observed after *sud1* silencing were partially suppressed by concomitant expression of a *perk* double-stranded RNA in the same disc compartment. $n \geq 30$ wings (*M*) and $n = 10$ wings (*N*) in three independent experiments. Error bars represent SD. One-way ANOVA analysis with Tukey comparison ($*P < 0.05$, $**P < 0.001$).

conserved, but context variable, biological role for Sud1/OGFOD1/Tpa1p in the regulation of growth and stress responses.

In flies, Sud1 suppression induces a strong UPR. Furthermore, partial suppression of the growth defects associated with *sud1* RNAi was observed with RNAi directed against *perk*, a key effector kinase in UPR signaling that targets eIF2α (35). Together, these findings suggest that the UPR is at least in part responsible for activation of stress pathways and impairment of growth related to Sud1. The observed induction of autophagy after *sud1* RNAi expression is also consistent with activation of UPR stress pathways. Despite similar effects on growth, eIF2α phosphorylation, and stress granule formation, induction of the UPR was not observed following OGFOD1 inactivation in mammalian cells (see ref. 22), suggesting the operation of additional signaling systems.

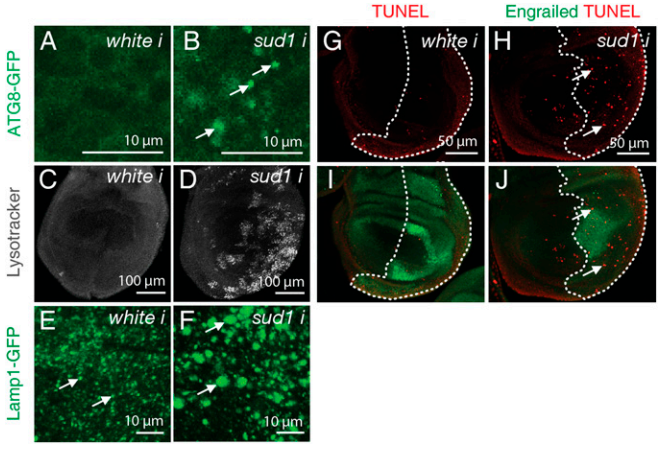

Fig. 5. Autophagy and apoptosis are induced after Sudestada1 knockdown. Expression of a *sud1* (*B*) but not of a *white* (control) (*A*) RNAi at the wing disc posterior compartment provokes nucleation of ATG8-GFP expressed at the same compartment, revealing that autophagy was induced. Autophagy induction was confirmed by Lysotracker-positive staining (*C* and *D*), as well as by nucleation of Lamp1-GFP (*E* and *F*) in cells of the same disc territory. Note in *E* and *F* that small Lamp1-GFP foci become bigger after *sud1* RNAi treatment. (*G–J*) Apoptosis is triggered after *sud1* silencing: Cells of the posterior wing disc compartment expressing *sud1* (*H* and *J*) but not those expressing a *white* (control) RNAi (*G* and *I*) become TUNEL positive (the arrows in *H* show two examples of TUNEL-positive cells). The posterior disc compartment that expresses Engrailed (green staining in *I* and *J*) is marked with a dotted line.

It has recently been reported that OGFOD1 is a stress granule component (20). In contrast with our findings in flies, in that report, OGFOD1 knockdown did not induce stress granule formation, suggesting that induction of translational stress is context determined. We observed suppressive effects of *sud1* RNAi on growth in both the fat body and wing disc compartments together with consistent effects on the induction of stress pathways in both developing flies and cultured *Drosophila* cells. By crossing in loss-of-function alleles of the TOR signaling pathway, and presumably reducing the rate of protein synthesis, growth defects provoked by *sud1* RNAi were partially suppressed, suggesting that translational stress was alleviated. Together with work in mammalian cells described in the accompanying manuscript (22), these results demonstrate that the activation of stress responses by OGFOD1/Sud1 knockdown occur in a number of settings. Nevertheless, as in mammalian and yeast cells, phenotypic responses to Sud1 suppression vary with context. For instance, the growth suppression was affected by nutritional supplementation, as addition of four times the quantity of yeast to the fly medium largely corrected the impairment in wing growth. Together with the effects in mouse embryonic fibroblasts being enhanced by transformation, it is possible that growth restriction by OGFOD1/Sud1 knockdown is enhanced in settings where there is an imbalance between growth and nutrient supply. We have thus far been unable to determine whether this reflects different effects on RPS23 hydroxylation or the downstream integration of signals on stress pathways.

Although there are differences between the effects of Sud1 and OGFOD1 knockdown in respect of the observed activation of the UPR, our results indicate that aspects of both the biochemical function of OGFOD1/Sud1 as ribosomal oxygenases and cellular functions in translational control and stress are conserved. Nevertheless, in other organisms, notably in the

BIOCHEMISTRY

fission yeast *S. pombe*, the homolog Ofd1 has a defined role as an oxygen sensor in the regulation of nuclear transcription by mediating oxygen-dependent proteolysis of Sre1, the homolog of sterol response element-binding proteins (SREBPs) (17, 18). Whether this response is conserved in flies is unclear. However, our analysis reveals that Sud1, like Tpa1p/OGFOD1, is a predominantly nuclear protein. An interesting possibility that will require exploration in future work is whether Sud1 functions in linking ribosomal signals, either generated at preribosomal stages before cytoplasmic export or from the assembled ribosome, to the regulation of nuclear transcriptional responses.

Currently the precise molecular mechanisms linking the growth/stress phenotypes observed in flies to RPS23 hydroxylation are unclear. This relationship is consistent with other studies in which defects in the production or metabolism of protein/nucleic acid components of the ribosome create cellular stress responses (36, 37). As described in refs. 21 and 22, the site of RPS23 hydroxylation is at the ribosomal decoding site and Tpa1p/OGFOD1 affects translation termination efficiency in yeast and mammalian cells.

In preliminary experiments measuring the effects of Sud1 knockdown on stop codon read through using a transgenic bicistronic reporter in *Drosophila*, we observed either no change or small increases in read through at different larval stages, indicating that general increases in stop codon readthrough are unlikely to be the sole Sud1-mediated signal activating the UPR. Nevertheless our results do not exclude the possibility that specific coding errors might be the activating signal, and this is the subject of future investigations.

Materials and Methods

Wing Size Measurement. Wings from 4-d-old females were removed and mounted in a solution containing 1:1 lactic acid/ethanol. Wings were imaged using an Olympus MVX10 stereomicroscope connected to an Olympus DP71 digital camera. The area of the posterior compartment was measured using ImageJ software (National Institutes of Health). To quantify the wing hairs, images were taken using an Olympus BX60 microscope connected to an Olympus DP71 digital camera.

Pupal Size Measurement. Pupae were photographed using the stereomicroscope as previously described. Pupal width and length were measured using Image J software. Volume was estimated using the following formula: $V = \pi D^2(3L - D)/12$, where D is the width and L the length of the pupa.

Fat Body Cell Nuclei Measurement. The area of fat body cell nuclei was measured using the ImageJ Software.

See *SI Materials and Methods* for additional information.

ACKNOWLEDGMENTS. We thank Ana Depetris Chauvin for help in statistical analyses, the Vienna Drosophila RNAi Centre (VDRC) and Bloomington Stock Centers, the many colleagues that provided *Drosophila* lines, the Hybridoma Bank for antibodies, and the Wappner laboratory members for discussion. This work was funded by Wellcome Trust Grant WT087675MA, Biotechnology and Biological Sciences Research Council UK, and Agencia Nacional de Promoción Científica y Tecnológica Grant 2011 N° 0090.

1. Loenarz C, Schofield CJ (2011) Physiological and biochemical aspects of hydroxylations and demethylations catalyzed by human 2-oxoglutarate oxygenases. *Trends Biochem Sci* 36(1):7–18.
2. Ozer A, Bruick RK (2007) Non-heme dioxygenases: Cellular sensors and regulators jelly rolled into one? *Nat Chem Biol* 3(3):144–153.
3. McDonough MA, Loenarz C, Chowdhury R, Clifton IJ, Schofield CJ (2010) Structural studies on human 2-oxoglutarate dependent oxygenases. *Curr Opin Struct Biol* 20(6):659–672.
4. Valegård K, et al. (1998) Structure of a cephalosporin synthase. *Nature* 394(6695):805–809.
5. Tsukada Y (2012) Hydroxylation mediates chromatin demethylation. *J Biochem* 151(3):229–246.
6. Loenarz C, Schofield CJ (2008) Expanding chemical biology of 2-oxoglutarate oxygenases. *Nat Chem Biol* 4(3):152–156.
7. DiTacchio L, et al. (2011) Histone lysine demethylase JARID1a activates CLOCK-BMAL1 and influences the circadian clock. *Science* 333(6051):1881–1885.
8. Herz HM, et al. (2010) The H3K27me3 demethylase dUTX is a suppressor of Notch- and Rb-dependent tumors in Drosophila. *Mol Cell Biol* 30(10):2485–2497.
9. Centanin L, Ratcliffe PJ, Wappner P (2005) Reversion of lethality and growth defects in Fatiga oxygen-sensor mutant flies by loss of hypoxia-inducible factor-alpha/Sima. *EMBO Rep* 6(11):1070–1075.
10. Jaakkola P, et al. (2001) Targeting of HIF-alpha to the von Hippel-Lindau ubiquitylation complex by O2-regulated prolyl hydroxylation. *Science* 292(5516):468–472.
11. Ivan M, et al. (2001) HIFalpha targeted for VHL-mediated destruction by proline hydroxylation: Implications for O2 sensing. *Science* 292(5516):464–468, Epub2001Apr.
12. Mecinović J, Loenarz C, Chowdhury R, Schofield CJ (2009) 2-Oxoglutarate analogue inhibitors of prolyl hydroxylase domain 2. *Bioorg Med Chem Lett* 19(21):6192–6195.
13. Leung IK, et al. (2013) Reporter ligand NMR screening method for 2-oxoglutarate oxygenase inhibitors. *J Med Chem* 56(2):547–555.
14. McDonough MA, et al. (2006) Cellular oxygen sensing: Crystal structure of hypoxia-inducible factor prolyl hydroxylase (PHD2). *Proc Natl Acad Sci USA* 103(26):9814–9819.
15. Henri J, et al. (2010) Structural and functional insights into Saccharomyces cerevisiae Tpa1, a putative prolylhydroxylase influencing translation termination and transcription. *J Biol Chem* 285(40):30767–30778.
16. Keeling KM, Salas-Marco J, Osherovich LZ, Bedwell DM (2006) Tpa1p is part of an mRNP complex that influences translation termination, mRNA deadenylation, and mRNA turnover in Saccharomyces cerevisiae. *Mol Cell Biol* 26(14):5237–5248.
17. Hughes BT, Espenshade PJ (2008) Oxygen-regulated degradation of fission yeast SREBP by Ofd1, a prolyl hydroxylase family member. *EMBO J* 27(10):1491–1501.
18. Lee CY, Yeh TL, Hughes BT, Espenshade PJ (2011) Regulation of the Sre1 hypoxic transcription factor by oxygen-dependent control of DNA binding. *Mol Cell* 44(2):225–234.
19. Saito K, Adachi N, Koyama H, Matsushita M (2010) OGFOD1, a member of the 2-oxoglutarate and iron dependent dioxygenase family, functions in ischemic signaling. *FEBS Lett* 584(15):3340–3347.
20. Wehner KA, Schütz S, Sarnow P (2010) OGFOD1, a novel modulator of eukaryotic translation initiation factor 2alpha phosphorylation and the cellular response to stress. *Mol Cell Biol* 30(8):2006–2016.
21. Loenarz C, et al. (2014) Hydroxylation of the eukaryotic ribosomal decoding center affects translational accuracy. *Proc Natl Acad Sci USA* 111:4019–4024.
22. Singleton RS, et al. (2014) OGFOD1 catalyses prolyl hydroxylation of RPS23 and is involved in translation control and stress granule formation. *Proc Natl Acad Sci USA* 111:4031–4036.
23. Kim HS, et al. (2010) Crystal structure of Tpa1 from Saccharomyces cerevisiae, a component of the messenger ribonucleoprotein complex. *Nucleic Acids Res* 38(6):2099–2110.
24. Delanoue R, Slaidina M, Léopold P (2010) The steroid hormone ecdysone controls systemic growth by repressing dMyc function in Drosophila fat cells. *Dev Cell* 18(6):1012–1021.
25. Colombani J, et al. (2003) A nutrient sensor mechanism controls Drosophila growth. *Cell* 114(6):739–749.
26. Lambertsson A (1998) The minute genes in Drosophila and their molecular functions. *Adv Genet* 38:69–134.
27. Lin JI, et al. (2011) Drosophila ribosomal protein mutants control tissue growth non-autonomously via effects on the prothoracic gland and ecdysone. *PLoS Genet* 7(12):e1002408.
28. Farny NG, Kedersha NL, Silver PA (2009) Metazoan stress granule assembly is mediated by P-eIF2alpha-dependent and -independent mechanisms. *RNA* 15(10):1814–1821.
29. Hetz C (2012) The unfolded protein response: Controlling cell fate decisions under ER stress and beyond. *Nat Rev Mol Cell Biol* 13(2):89–102.
30. Ryoo HD, Domingos PM, Kang MJ, Steller H (2007) Unfolded protein response in a Drosophila model for retinal degeneration. *EMBO J* 26(1):242–252.
31. Kroemer G, Mariño G, Levine B (2010) Autophagy and the integrated stress response. *Mol Cell* 40(2):280–293.
32. Scott RC, Juhász G, Neufeld TP (2007) Direct induction of autophagy by Atg1 inhibits cell growth and induces apoptotic cell death. *Curr Biol* 17(1):1–11.
33. Wullschleger S, Loewith R, Hall MN (2006) TOR signaling in growth and metabolism. *Cell* 124(3):471–484.
34. Ge W, et al. (2012) Oxygenase-catalyzed ribosome hydroxylation occurs in prokaryotes and humans. *Nat Chem Biol* 8(12):960–962.
35. Pomar N, et al. (2003) Functional characterization of Drosophila melanogaster PERK eukaryotic initiation factor 2alpha (eIF2alpha) kinase. *Eur J Biochem* 270(2):293–306.
36. Boglev Y, et al. (2013) Autophagy induction is a Tor- and Tp53-independent cell survival response in a zebrafish model of disrupted ribosome biogenesis. *PLoS Genet* 9(2):e1003279.
37. Danilova N, Sakamoto KM, Lin S (2008) Ribosomal protein S19 deficiency in zebrafish leads to developmental abnormalities and defective erythropoiesis through activation of p53 protein family. *Blood* 112(13):5228–5237.

Supporting Information

Katz et al. 10.1073/pnas.1314485111

SI Materials and Methods

Fly Stocks. Flies used in this study were *yw*, w^{1118}, *en*-Gal4, *actin*-Gal4, *btl*-Gal4, *nub*-Gal4, *pumpless*-Gal4 (*ppl*-Gal4), *ms1096*-Gal4, UAS-p35, UAS-GFP, $thor^2$ (1), and *wRNAi* from the Bloomington *Drosophila* stock center (http://flystocks.bio.indiana.edu); *sud1* RNAi (#3402), UAS-DicerII, and *perk* RNAi (#110278) from the Vienna Drosophila RNAi Center (VDRC, http://stockcenter.vdrc.at/control/main); *btl*-Gal4 (2); and *ldh*-LacZ (3). UAS-Xbp1-GPF was a gift from Hermann Steller (The Rockefeller University, New York) (4). Helmut Kramer (University of Texas Southwestern Medical Center, Dallas) kindly provided the UAS-LAMP1-GFP line (5). UAS-ATG8-GFP was kindly provided by Thomas Neufeld (University of Minnesota, Minneapolis) (6). $rheb^{P\Delta1}$, $rheb^{P\Delta2}$ (7), TSC^{Q87X} (8), TOR^{2L1} (9), and $S6K^{L1}$ (10) were kindly provided by Sean Oldham (Sanford-Burnham Medical Research Institute, La Jolla, CA). In all experiments throughout this study, larvae were synchronized 24 h after egg deposition and grown at a controlled density (50 larvae per vial) in standard culture media at 25 °C or 29 °C depending on the experiment.

Cloning and Transgenic Lines Generation. Transgenic lines bearing the UAS-hOGFOD, UAS-wSud1, and bicistronic luciferase reporter were generated by phiC31-mediated site-directed integration on the 86F platform. The UAS-GFP-Sud1 was generated using the P element–mediated transformation method (11).

For the generation of the pUASt-wSud1 construct, the ORF of wSudestada was amplified by PCR from *Drosophila willistoni* females (EHIME University) cDNA using the following primers: 5′-GGAAGATCTATGGACACGGCCGAATCCAC-3′ and 5′-AAGGAAAAAAGCGGCCGCTTACTCCTTGTAACTACATGACATC-3′. The amplified fragment was subcloned into the pCR 2.1 TOPO vector (Invitrogen #45-0641) and was then cloned into the pUASt attb vector using KpnI and XhoI restriction sites. The ORF from hOGFOD was subcloned into the pUASt attb using the BamHI and XbaI restriction sites.

For the generation of the UAS-GFP-Sud1 construct, the Sud1 ORF was amplified by PCR from the first-instar larvae cDNA template using the following primers: 5′-CACCATGGAAACCTCGAGCT-3′ and 5′-CTACTCCTTGTAGCTGCACGAAAT-3′. The amplified fragment was subcloned using the pENTR/D-Topo clonig kit (Invitrogen #45-0218) and then cloned into the gateway pTGW expression plasmid.

N-terminally truncated human $RPS23_{44–143}$ was cloned into a bacterial expression vector providing an *N*-terminal GST-tag. Full-length *Drosophila melanogaster* Sudestada1 was cloned into the pET-28a vector with the *N*-terminal His_6-tag from CG44254 cDNA (isoform A) on the pUAS.g attb plasmid.

Real-Time PCR. Total RNA was isolated using the TRIzol reagent (Invitrogen). Genomic DNA was removed from RNA samples using the Ambion's DNA free kit. RNAs (1–1.5 μg) were reverse-transcribed using the superscript III First-strand synthesis system (Invitrogen) and oligo-dT as a primer. The resulting cDNA was used for real-time PCR (Stratagene MX300 sp), using Taq DNA polymerase (Invitrogen) and SYBRGreen and ROX (Invitogen) as fluorescent dyes. *Sud*- and *Bip*-specific primers were used. Samples were normalized using *tub* primers. Three independent biological samples were analyzed in each experiment. One representative set of results is shown for each experiment. Primer sequences were as follows: *Sud2* Fw, GCCAGTTGCTCATCGCCGAACT; *Sud2* Rv, GCGTGTGTGCTTCCTGGGTCA; *Sud1* Fw, GGTCGCAGCTGTTGGCCGAT; *Sud1* Rv, GTGGGACCAGCGCTGCAGTT; *Bip* Fw, GGCATTGATTTGGGCACCACGTAT; *Bip* Rv, TGTTCTCGGGATTGGTGGTCAACT; *Tub* Fw, ATCCCCAACAACGTGAAGAC; *Tub* Rv, GCCTGAACATAGCGGTGAAC.

Antibody Staining. Larvae were dissected in PBS and then fixed in 4% (vol/vol) formaldehyde (Sigma) for 40 min (imaginal discs) or 2 h (fat body) at room temperature, and samples were then washed in PT (PBS + 0.3% Triton X-100) for the imaginal discs or PBST (PBS + 0.1% Tween-20) for the fat bodies. Thereafter, samples were incubated for 2 h in PT + 5% (wt/vol) BSA (PBT) and then incubated with the primary antibody in PBT for 2 h at room temperature or overnight at 4 °C. Tissues were then washed three times for 20 min and incubated for another 2 h at room temperature with the secondary antibody diluted in PT + 5% (vol/vol) normal goat serum + 300 nM DAPI. After washing, imaginal discs were separated and mounted in 80% (vol/vol) glycerol.

The primary antibodies used were mouse anti-Engrailed (Developmental Studies Hybridoma Bank—DSHB 4D9; 1/100), rabbit anti-P-eIf2α (Cell Signaling #9721; 1/100), and rabbit anti-GFP (Molecular Probes #6455; 1/1,000). Secondary antibodies were donkey anti-rabbit Cy2 (Jackson #711–225-152), goat anti-rabbit Cy3 (Jackson #111–165-144), and donkey anti-mouse Cy3 (Jackson #715–165-150).

For phalloidin and DAPI stainings, larvae were dissected, fixed, and washed in PBST, after which they were incubated for 1 h at room temperature in 0.165 μM Alexa Fluor 488 phalloidin in PT or PBST containing 300 nM DAPI. After several washes, tissues or organs were sorted and mounted in 80% glycerol.

Lysotracker staining and TUNEL analysis were carried out as previously described (12, 13).

Wing Discs DTT Treatments. Larvae were dissected and incubated for 4 h in Schneider medium containing 5 mM DTT. Imaginal discs were then used for anti-GFP immunostainings.

Cell Culture. *Drosophila* Schneider's line $S2R^+$ cells were maintained at 28 °C in Schneider media (Sigma) and supplemented with 10% (vol/vol) FBS (Gibco), 50 U/mL penicillin, and 50 μg/mL streptomycin in 75-cm^2 T-flasks (Greiner).

dsRNA Synthesis and S2 Cell RNAi Treatment. A fragment of the *sud1* gene was amplified by PCR from cDNA using T7-tailed oligonucleotides as primers [primer sequence: *Drosophila* RNAi Screening Centre (www.flyrnai.org/DRSC-DRS.html) #15388]. dsRNA was synthetized using the T7 Megascript kit (Ambion). The bathing method was used to introduce dsRNAs into the cells as previously described (14). Cells were incubated with the dsRNA for 5 d. For stress granule assays, 0.25 mM sodium arsenite was added to the medium for 2 h before the samples were processed.

Stress granule detection. Stress granules (SGs) in *Drosophila* $S2R^+$ cells were visualized by FISH for polyadenylated RNA using oligodT-Cy3 (Sigma), as previously indicated (15). The granules were analyzed automatically with the BUHO MATLAB script as previously described (16).

β-Galactosidase assay. For X-Gal stainings, embryos were dechorionated and fixed with 0.5% glutaraldehyde for 20 min. Embryos were then washed with PBST and incubated at 37 °C with the β-galactosidase synthetic substrate X-gal.

Western Blots. Western blots were carried out by standard procedures using ECL plus (GE, RPN2232). The primary antibodies used were rabbit anti-P-eIf2α (Cell Signaling #9721; 1/1,000) and anti–α Tubulin (Developmental Studies Hybridoma Bank—DSHB;

http://dshb.biology.uiowa.edu; 12G10; 1/10,000). Secondary peroxidase–conjugated antibodies used were donkey anti-mouse (Jackson ImmunoResearch #715-035-150; 1/5,000) and donkey anti-rabbit (Jackson ImmunoResearch #111-035-144; 1/5,000).

Protein Synthesis Assay. Forty wing imaginal discs were dissected and incubated in a custom-made L-amino acid mixture [^{14}C(U)] containing alanine, arginine, glutamic acid, lysine, and serine (Perkin-Elmer) for 30 min. The supernatant was then removed, and tissues were washed in PBS and lysed in RIPA buffer. Trichloroacetic acid–insoluble radioactivity relative to total radioactivity in the lysates was evaluated in duplicate measurements.

Whole-Protein MS of Ribosomal Proteins. Ribosomal protein masses were analyzed by reversed phase ultra-performance liquid chromatography (RP-UPLC) and electrospray ionization time-of-flight mass spectrometry (ESI-TOF MS). The method used a Waters BEH C4 reversed phase column (2.1 × 50 mm, 1.7-μm particle size, 300-Å pore size). A flow rate of 0.3 mL/min was used with the column held at 40 °C using a Waters Acquity UPLC system connected directly to a Waters LCT ESI-TOF MS. The column was equilibrated with solvent A (0.1% formic acid in water). Five microliters of ribosomal protein sample was injected onto the column, and proteins were eluted using a stepped gradient from solvent A to solvent B (0.1% formic acid in acetonitrile). The following MS parameters were used: polarity, ES+; capillary voltage, 3,000 V; Sample cone voltage, 35 V; desolvation temperature, 250 °C; cone gas flow rate, 30 L/h; desolvation gas flow (N_2), 500 L/h. The mass spectra were acquired from 420 to 2,500 *m/z* using MassLynx 4.1 software (Waters), and protein spectra were deconvoluted using Maxent 1 with a range of 3–30 kDa (0.1-Da resolution). Masses were confirmed using manual component analysis. Sodium formate was used for instrument calibration, and leucine enkephalin was used as the lockspray compound allowing online mass correction.

LC-MS/MS Protein Analysis. LC-MS/MS analysis of the digested material was initially performed on an Agilent 6520 Q-TOF mass analyzer after separation on a 43-mm × 75-μm Zorbax 300SB-C18 5-μm chip column (Agilent) using a 23-min gradient of 5–40% solvent B (solvent A: 2% MeCN, 0.1% HCOOH; solvent B: 95% MeCN, 0.1% HCOOH). Further analysis of selected biological samples were carried out by nano-ultra performance liquid chromatography tandem MS (nano-UPLC-MS/MS) using a 75-μm inner diameter × 25-cm C18 nanoAcquity UPLC column (1.7-μm particle size; Waters) with a 45-min gradient of 2–40% solvent B (solvent A: 99.9% H_2O, 0.1% HCOOH; solvent B: 99.9% MeCN, 0.1% HCOOH). The Waters nanoAcquity UPLC system (final flow rate, 250 nl/min; ~7,000 psi) was coupled to a Q-TOF Premier tandem mass spectrometer (Waters) run in positive ion mode. MS analysis was performed in data-directed analysis (DDA) mode with MS to MS/MS switching at precursor ion counts greater than 10 with a return from MS/MS to MS survey after 1 s (MS/MS collision energy is dependent on precursor ion mass and charge state). All raw MS data were processed using either the MassHunter Qualitative Analysis version B.01.03 (Agilent) or PLGS version 2.3 (Waters) software with deisotoping and deconvolution (converting masses with multiple charge states to $m/z = 1$). The mass accuracy of the raw data were corrected using Glu-fibrinopeptide for the Waters QTOF and the background ion from dodecamethylcyclohexasiloxane at 445.12 Da for the Agilent QTOF. MS/MS spectra of the digested biological samples (Agilent, mgf files; Waters, pkl files) were searched against the UniProtKB/Swiss-Prot database (version 2010.08.13; 519,348 sequences) database using Mascot version 2.3.01 (Matrix Science) with the following parameters: peptide tolerance, 0.2 Da; $^{13}C = 1$; fragment tolerance, 0.1 Da; missed cleavages, 2; instrument type, ESI-Q-TOF-IMM; fixed modification, carbamidomethylation (C); and variable modifications, deamidation (Asp, Glu), oxidation (Met, Asn, Pro), and dioxidation (Pro). All database searches were performed on human or the corresponding species' entries. Assignments of hydroxylation on sites identified by Mascot were verified by manual inspection. MS/MS spectra were processed for documentation using the MassHunter Qualitative Analysis and MassLynx (v. 4.1) software for the Agilent and Waters data, respectively.

Protein Expression, Purification, and Coexpression Studies. Proteins were heterologously expressed using *Escherichia coli* BL21-DE3 cells and purified with Äkta FPLC systems. Expression was induced by isopropyl-β-D-thiogalactosidase (typically 0.5 mM, ~14 h at 18 °C) before harvest. GST-RPS23$_{44–143}$ was expressed either alone (control) or coexpressed together with His$_6$-Sudestada1, and then lysed (200 mM NaCl in 50 mM Tris, pH 7.5) by sonication and purified using immobilized glutathione agarose affinity, followed by in-solution trypsinolysis.

1. Bernal A, Kimbrell DA (2000) Drosophila Thor participates in host immune defense and connects a translational regulator with innate immunity. *Proc Natl Acad Sci USA* 97(11):6019–6024.
2. Shiga YT-MM, Hayashi S (1996) A nuclear GFP/β-galactosidase fusion protein as a marker for morphogenesis in living Drosophila. *Dev Growth Differ* 38(1):99–106.
3. Lavista-Llanos S, et al. (2002) Control of the hypoxic response in Drosophila melanogaster by the basic helix-loop-helix PAS protein similar. *Mol Cell Biol* 22(19): 6842–6853.
4. Ryoo HD, Domingos PM, Kang MJ, Steller H (2007) Unfolded protein response in a Drosophila model for retinal degeneration. *EMBO J* 26(1):242–252.
5. Pulipparacharuvil S, et al. (2005) Drosophila Vps16A is required for trafficking to lysosomes and biogenesis of pigment granules. *J Cell Sci* 118(Pt 16):3663–3673.
6. Arsham AM, Neufeld TP (2009) A genetic screen in Drosophila reveals novel cytoprotective functions of the autophagy-lysosome pathway. *PLoS ONE* 4(6):e6068.
7. Zhang Y, et al. (2003) Rheb is a direct target of the tuberous sclerosis tumour suppressor proteins. *Nat Cell Biol* 5(6):578–581.
8. Tapon N, Ito N, Dickson BJ, Treisman JE, Hariharan IK (2001) The Drosophila tuberous sclerosis complex gene homologs restrict cell growth and cell proliferation. *Cell* 105(3):345–355.
9. Oldham S, Montagne J, Radimerski T, Thomas G, Hafen E (2000) Genetic and biochemical characterization of dTOR, the Drosophila homolog of the target of rapamycin. *Genes Dev* 14(21):2689–2694.
10. Gao X, et al. (2002) Tsc tumour suppressor proteins antagonize amino-acid-TOR signalling. *Nat Cell Biol* 4(9):699–704.
11. Bateman JR, Lee AM, Wu CT (2006) Site-specific transformation of Drosophila via phiC31 integrase-mediated cassette exchange. *Genetics* 173(2):769–777.
12. Milán M, Campuzano S, García-Bellido A (1996) Cell cycling and patterned cell proliferation in the wing primordium of Drosophila. *Proc Natl Acad Sci USA* 93(2): 640–645.
13. Scott RC, Juhász G, Neufeld TP (2007) Direct induction of autophagy by Atg1 inhibits cell growth and induces apoptotic cell death. *Curr Biol* 17(1):1–11.
14. Clemens JC, et al. (2000) Use of double-stranded RNA interference in Drosophila cell lines to dissect signal transduction pathways. *Proc Natl Acad Sci USA* 97(12): 6499–6503.
15. Loschi M, Leishman CC, Berardone N, Boccaccio GL (2009) Dynein and kinesin regulate stress-granule and P-body dynamics. *J Cell Sci* 122(Pt 21):3973–3982.
16. Perez-Pepe M, et al. (2012) BUHO: A MATLAB script for the study of stress granules and processing bodies by high-throughput image analysis. *PLoS ONE* 7(12):e51495.

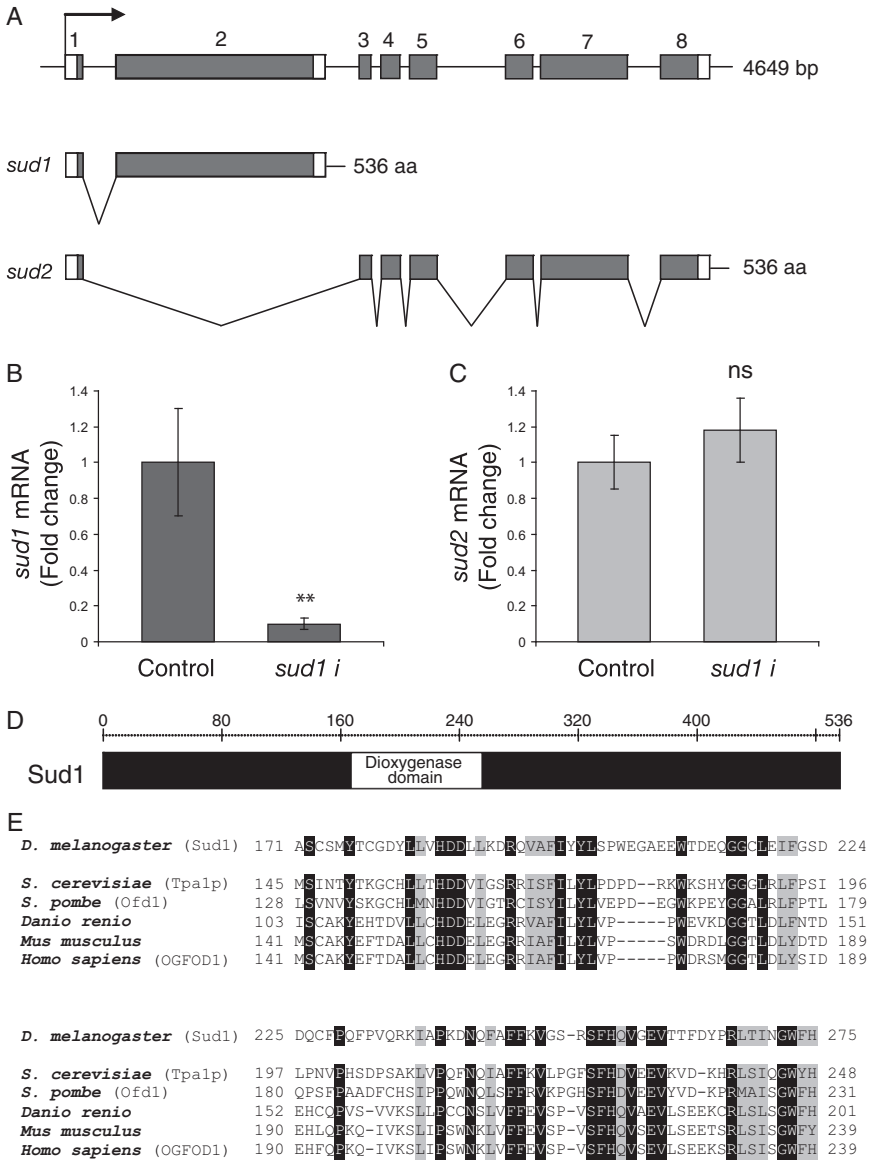

Fig. S1. The *sudestada* locus and RNAi-mediated silencing of *sud1* and *sud2* transcripts. (*A*) The locus *sudestada* (CG44254; www.flybase.org) encompasses eight exons and gives rise to two transcripts by alternative splicing, *sud1* and *sud2*, that have in common only exon 1. (*B* and *C*) *sudestada1* (*sud1*) and *sudestada2* (*sud2*) transcript levels were determined by qRT-PCR from total RNA extracted from first-instar larvae that express a *sud1* or a *white* (control) double-stranded RNA driven by *actin*-Gal4 in transgenic flies. Whereas *sud1* RNAi suppresses *sud1* transcript levels to less than 10% of control levels, the same RNAi does not affect *sud2* transcript levels. Error bars represent SD. (*D*) Sud1 protein includes a putative dioxygenase domain encoded by exon 2. (*E*) The *Drosophila* Sud1 dioxygenase domain is highly conserved in evolution. Identical amino acid residues are marked in black; amino acid residues displaying similarity between species are shown in gray.

Fig. S2. Sud1 silencing in the tracheal system and dorsal wing compartment. (*A–D*) Sud1 knockdown in the tracheal system does not affect HIF signaling in this tissue, as determined by the expression of an *ldh*-lacZ hypoxia inducible reporter in transgenic embryos, visualized by X-Gal staining. (*A*) Embryos expressing a *white* (control) double stranded RNA driven by *breathless*-Gal4 do not express the reporter in mild hypoxia (8% O_2). (*B*) The same embryos exposed to 5% O_2 display strong expression of the hypoxia-inducible reporter in tracheal cells (arrows). (*C*) Embryos exposed to mild hypoxia (8% O_2) and expressing a *fatiga* (*fga*) double stranded RNA under control of a *breathless*-Gal4 driver exhibit strong activation of the reporter in a pattern similar to that observed in *B* (arrows). (*D*) Embryos at 8%O_2 expressing *sud1* RNAi in the tracheal system do not activate the reporter, suggesting that Sud1 silencing does not activate HIF signaling. *sud1* (*E*) or *white* (control) (*F*) double-stranded RNAs were expressed in the wing disc dorsal compartment using a *ms1096*-Gal4 driver. Wings of flies expressing *sud1* but not a control RNAi are bended upward, indicating that the wing dorsal cell layer is smaller than the ventral layer. This wing phenotype implies that Sud1 silencing provokes growth impairment in this experimental setting.

A

GIVLEKYGVEAKQP (+15.99)NSAIR

Identified in MSS6793 1 x Oxidation (P)
Charge: 3, Exp. m/z: 675.388, Calc. m/z: 675.387

Max Intensity: 1.51 e+03

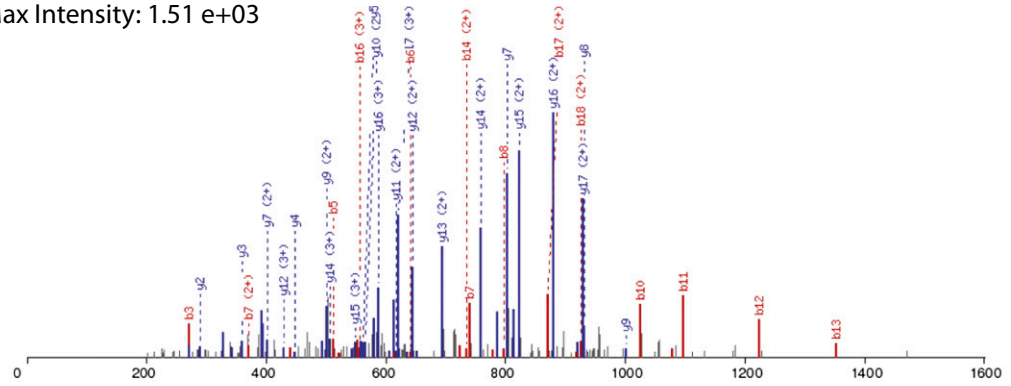

Key:	m/z out of range of spectrum	matched c-term ion	unmatched c-term ion	matched n-term ion	unmatched n-term ion

	G	I	V	L	E	K	V	G	V	E	A	K	Q	P	N	S	A	I	
	1	2	3	4	5	6	7	8	9	10	11	12	13	14	15	16	17	18	
a		143.12																	a
b		171.11	270.18	383.27	512.31	640.40	739.47	796.49	895.56	1024.60	1095.64	1223.74	1351.79	1464.84	1578.88	1665.92	1736.95	1850.04	b
b–15.99														1448.85	1562.89	1649.92	1720.96	1834.04	b–15.99
b (2+)						320.71	370.24	398.75	448.28	512.81	548.32	612.37	676.40	732.92	789.95	833.46	868.98	925.52	b (2+)
b–15.99 (2+)														724.93	781.95	825.46	860.98	917.53	b–15.99 (2+)
b (3+)												408.58	451.27	488.95	526.97	555.98	579.66	617.35	b (3+)
b–15.99 (3+)														483.62	521.63	550.65	574.32	612.02	b–15.99 (3+)
y		1967.13	1854.04	1754.98	1641.89	1512.85	1384.75	1285.69	1228.66	1129.60	1000.55	929.52	801.42	673.36	560.32	446.27	359.24	288.20	y
y–15.99		1951.13	1838.05	1738.98	1625.90	1496.85	1368.76	1269.69	1212.67	1113.60	984.56	913.52	785.43	657.37					y–15.99
y (2+)		984.07	927.53	877.99	821.45	756.93	692.88	643.35	614.84	565.30	500.78	465.26	401.21	337.19	280.66	223.64	180.12	144.61	y (2+)
y–15.99 (2+)		976.07	919.53	869.99	813.45	748.93	684.88	635.35	606.84	557.30	492.78	457.26	393.22	329.19					y–15.99 (2+)
y (3+)		656.38	618.69	585.66	547.97	504.95	462.26	429.23	410.23	377.20	334.19	310.51							y (3+)
y–15.99 (3+)		651.05	613.35	580.33	542.64	499.62	456.92	423.90	404.89	371.87	328.86	305.18							y–15.99 (3+)
	G	I	V	L	E	K	V	G	V	E	A	K	Q	P	N	S	A	I	
	19	18	17	16	15	14	13	12	11	10	9	8	7	6	5	4	3	2	

	R	
	19	
a		a
b		b
b–15.99		b–15.99
b (2+)		b (2+)
b–15.99 (2+)		b–15.99 (2+)
b (3+)		b (3+)
b–15.99 (3+)		b–15.99 (3+)
y	175.12	y
y–15.99		y–15.99
y (2+)	88.06	y (2+)
y–15.99 (2+)		y–15.99 (2+)
y (3+)		y (3+)
y–15.99 (3+)		y–15.99 (3+)
	R	
	1	

Fig. S3. (Continued)

B
GIVLEKYGVEAKQP (+15.99)NSAIR

Identified in MSS6793 1 x Oxidation (P)
Charge: 3, Exp. m/z: 675.389, Calc. m/z: 675.387

Max Intensity: 1.49 e+03

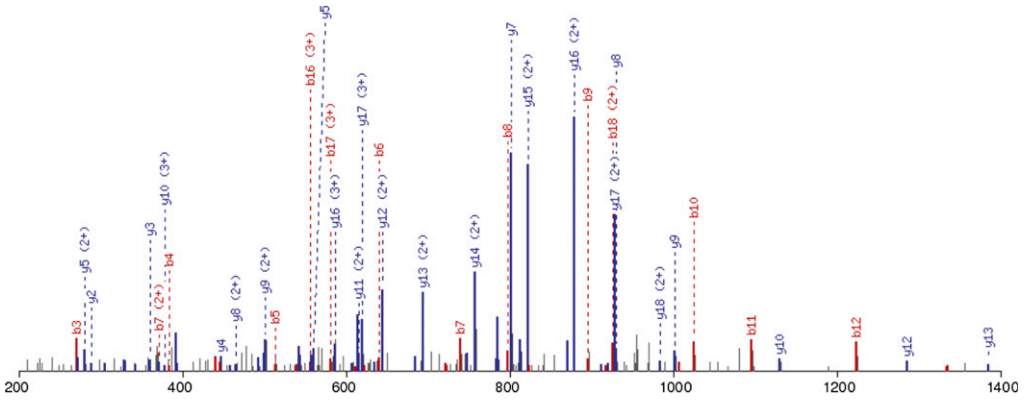

Key: m/z out of range of spectrum | matched c-term ion | unmatched c-term ion | matched n-term ion | unmatched n-term ion

	G	I	V	L	E	K	V	G	V	E	A	K	Q	P	N	S	A	I	
	1	2	3	4	5	6	7	8	9	10	11	12	13	14	15	16	17	18	
a		143.12																	a
b		171.11	270.18	383.27	512.31	640.40	739.47	796.49	895.56	1024.60	1095.64	1223.74	1351.79	1464.84	1578.88	1665.92	1736.95	1850.04	b
b--15.99														1448.85	1562.89	1649.92	1720.96	1834.04	b--15.99
b (2+)						320.71	370.24	398.75	448.28	512.81	548.32	612.37	676.40	732.92	789.95	833.46	868.98	925.52	b (2+)
b--15.99 (2+)														724.93	781.95	825.46	860.98	917.53	b--15.99 (2+)
b (3+)												408.58	451.27	488.95	526.97	555.98	579.66	617.35	b (3+)
b--15.99 (3+)														483.62	521.63	550.65	574.32	612.02	b--15.99 (3+)
y		1967.13	1854.04	1754.98	1641.89	1512.85	1384.75	1285.69	1228.66	1129.60	1000.55	929.52	801.42	673.36	560.32	446.27	359.24	288.20	y
y--15.99		1951.13	1838.05	1738.98	1625.90	1496.85	1368.76	1269.69	1212.67	1113.60	984.56	913.52	785.43	657.37					y--15.99
y (2+)		984.07	927.53	877.99	821.45	756.93	692.88	643.35	614.84	565.30	500.78	465.26	401.21	337.19	280.66	223.64	180.12	144.61	y (2+)
y--15.99 (2+)		976.07	919.53	869.99	813.45	748.93	684.88	635.35	606.84	557.30	492.78	457.26	393.22	329.19					y--15.99 (2+)
y (3+)		656.38	618.69	585.66	547.97	504.95	462.26	429.23	410.23	377.20	334.19	310.51							y (3+)
y--15.99 (3+)		651.05	613.35	580.33	542.64	499.62	456.92	423.90	404.89	371.87	328.86	305.18							y--15.99 (3+)
	G	I	V	L	E	K	V	G	V	E	A	K	Q	P	N	S	A	I	
	19	18	17	16	15	14	13	12	11	10	9	8	7	6	5	4	3	2	

	R	
	19	
a		a
b		b
b--15.99		b--15.99
b (2+)		b (2+)
b--15.99 (2+)		b--15.99 (2+)
b (3+)		b (3+)
b--15.99 (3+)		b--15.99 (3+)
y	175.12	y
y--15.99		y--15.99
y (2+)	88.06	y (2+)
y--15.99 (2+)		y--15.99 (2+)
y (3+)		y (3+)
y--15.99 (3+)		y--15.99 (3+)
	R	
	1	

Fig. S3. (Continued)

C

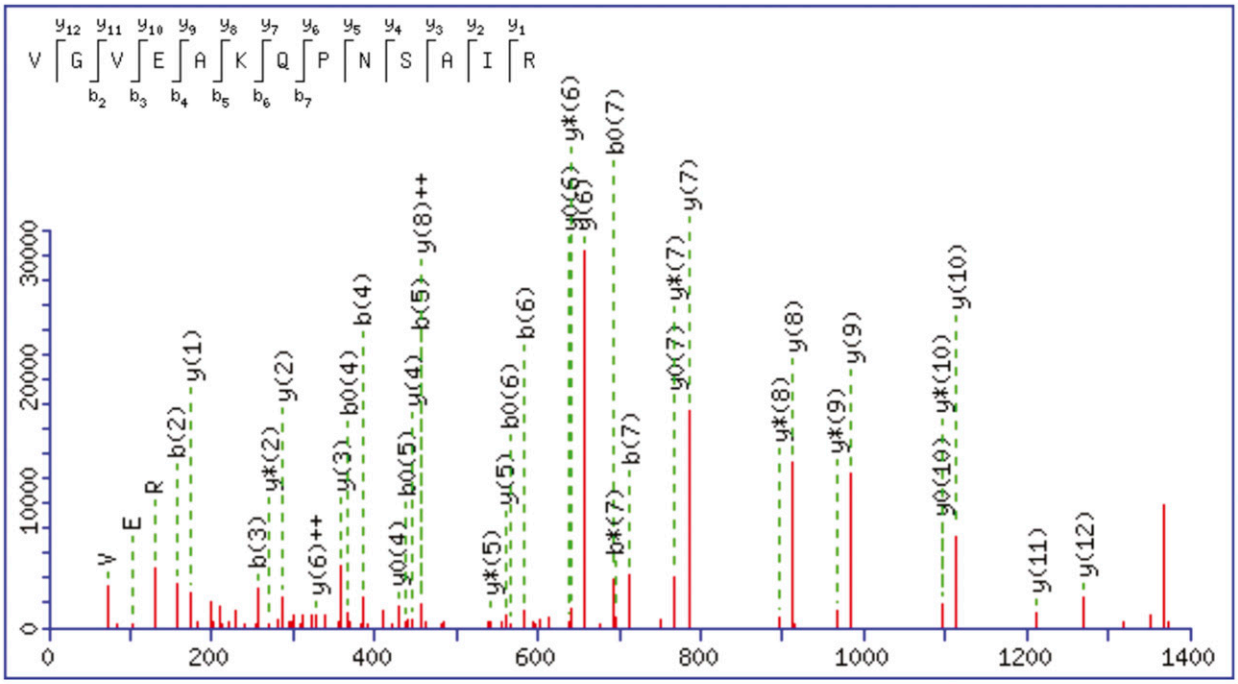

D

#	Immon.	b	b^{++}	b*	b^{*++}	b^0	b^{0++}	Seq.	y	y^{++}	y*	y^{*++}	y^0	y^{0++}	#
1	**72.0808**	100.0757	50.5415					V							13
2	30.0338	**157.0972**	79.0522					G	**1269.6910**	635.3491	1252.6644	626.8359	1251.6804	626.3438	12
3	**72.0808**	**256.1656**	128.5864					V	**1212.6695**	606.8384	1195.6430	598.3251	1194.6589	597.8331	11
4	**102.0550**	**385.2082**	193.1077			**367.1976**	184.1024	E	**1113.6011**	557.3042	**1096.5745**	548.7909	**1095.5905**	548.2989	10
5	44.0495	**456.2453**	228.6263			**438.2347**	219.6210	A	**984.5585**	492.7829	**967.5320**	484.2696	966.5479	483.7776	9
6	101.1073	**584.3402**	292.6738	567.3137	284.1605	**566.3297**	283.6685	K	**913.5214**	**457.2643**	**896.4948**	448.7511	895.5108	448.2591	8
7	101.0709	**712.3988**	356.7030	**695.3723**	348.1898	**694.3883**	347.6978	Q	**785.4264**	393.2169	**768.3999**	384.7036	**767.4159**	384.2116	7
8	70.0651	809.4516	405.2294	792.4250	396.7162	791.4410	396.2241	P	**657.3678**	**329.1876**	**640.3413**	320.6743	**639.3573**	320.1823	6
9	87.0553	923.4945	462.2509	906.4680	453.7376	905.4839	453.2456	N	**560.3151**	280.6612	**543.2885**	272.1479	542.3045	271.6559	5
10	60.0444	1010.5265	505.7669	993.5000	497.2536	992.5160	496.7616	S	**446.2722**	223.6397	429.2456	215.1264	**428.2616**	214.6344	4
11	44.0495	1081.5636	541.2855	1064.5371	532.7722	1063.5531	532.2802	A	**359.2401**	180.1237	342.2136	171.6104			3
12	86.0964	1194.6477	597.8275	1177.6212	589.3142	1176.6371	588.8222	I	**288.2030**	144.6051	**271.1765**	136.0919			2
13	**129.1135**							R	**175.1190**	88.0631	158.0924	79.5498			1

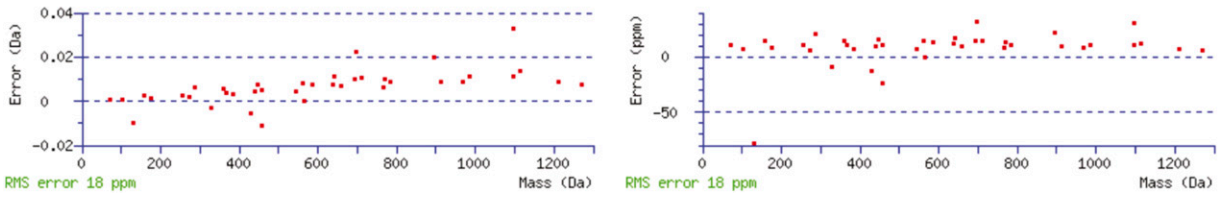

Fig. S3. (Continued)

E

#	Immon.	b	b^{++}	b*	b^{*++}	b^{0}	b^{0++}	Seq.	y	y^{++}	y*	y^{*++}	y^{0}	y^{0++}	#
1	**72.0808**	100.0757	50.5415					V							13
2	30.0338	**157.0972**	79.0522					G	**1285.6859**	**643.3466**	1268.6593	634.8333	1267.6753	634.3413	12
3	**72.0808**	**256.1656**	128.5864					V	**1228.6644**	614.8359	1211.6379	606.3226	1210.6539	605.8306	11
4	**102.0550**	**385.2082**	193.1077			**367.1976**	184.1024	E	**1129.5960**	**565.3016**	1112.5695	**556.7884**	**1111.5854**	**556.2964**	10
5	44.0495	**456.2453**	228.6263			**438.2347**	219.6210	A	**1000.5534**	500.7803	**983.5269**	492.2671	982.5429	491.7751	9
6	**101.1073**	**584.3402**	292.6738	567.3137	284.1605	566.3297	283.6685	K	**929.5163**	465.2618	**912.4898**	456.7485	911.5057	**456.2565**	8
7	**101.0709**	**712.3988**	356.7030	**695.3723**	348.1898	694.3883	347.6978	Q	**801.4213**	401.2143	**784.3948**	392.7010	**783.4108**	392.2090	7
8	86.0600	825.4465	413.2269	808.4199	404.7136	807.4359	404.2216	P	**673.3628**	337.1850	**656.3362**	328.6717	**655.3522**	**328.1797**	6
9	87.0553	939.4894	470.2483	922.4629	461.7351	921.4789	461.2431	N	**560.3151**	280.6612	**543.2885**	272.1479	542.3045	271.6559	5
10	60.0444	1026.5215	513.7644	1009.4949	505.2511	1008.5109	504.7591	S	**446.2722**	223.6397	**429.2456**	215.1264	**428.2616**	214.6344	4
11	44.0495	1097.5586	549.2829	1080.5320	540.7696	1079.5480	540.2776	A	**359.2401**	180.1237	342.2136	171.6104			3
12	86.0964	1210.6426	605.8250	1193.6161	597.3117	1192.6321	596.8197	I	**288.2030**	144.6051	**271.1765**	136.0919			2
13	**129.1135**							R	**175.1190**	88.0631	158.0924	79.5498			1

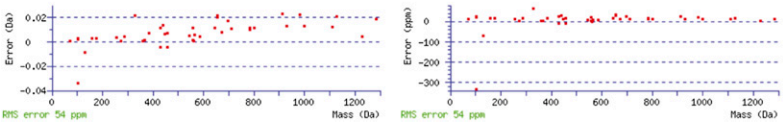

Fig. S3. Tandem MS assignment of Arg-C peptide species (*m/z* 675.388) as hydroxylated [M+3H]3+ RPS23 peptide amino acids 49–67. (*A* and *B*) Database search of the *m/z* 675.388 species detected by LC-MS/MS in the retention time range of 37.5 min assigns the peptide species with statistical significance as being GIVLEKVGVEAKQPNSAIR from RPS23, carrying a 16-Da mass increment (hydroxylation) on either Gln-61 or Pro-62. The fragment ion mass corresponding to the y6 ion (673.36 Da), which would formally assign Pro-62 as the site of modification, is not recorded by the ion trap mass analyzer. However, coverage of the remaining y-ions, ranging from the y2 ion to the y11 ion indicates a 16-Da mass shift on the adjacent y7 fragment ion, localizing the modification to Gln-61 or Pro-62. Formal (unambiguous) assignment of Pro-62 hydroxylation on a related peptide is provided in Fig. 3*E*. MS/MS assignment of *m/z* 670.057 was not possible owing to the low abundance of the precursor ion. However, the exact mass and retention time of the *m/z* 670.057 species are consistent with the unmodified peptide GIVLEKVGVEAKQPNSAIR (which is identical in human rpS23) and formally assigned in a companion article. (*C*) LC-MS/MS analysis of trypsinized GST-RPS23. In the absence of Sudestada1, RPS23 Pro-62 was unmodified (control experiment for data reported in Fig. 3*E*). The b and y fragment ions are indicated (peptide precursor ion: M_r 1,367.691848 Da; calculated 1,367.7521 Da). (*D*) Tables of observed MS/MS fragment ions of trypsinized GST-RPS23 depicted in *C*. Control experiment of RPS23 55-VGVEAKQPNSAIR-67 lacking modification at Pro-62. (*E*) Tables of observed MS/MS fragment ions of trypsinized GST-RPS23 depicted in Fig. 3*E*. RPS23 55-VGVEAKQPNSAIR-67 monohydroxylated (+16 Da) at Pro-62 after coexpression with His6-Sudestada1. The table lists the b, y, and immonium fragment ions.

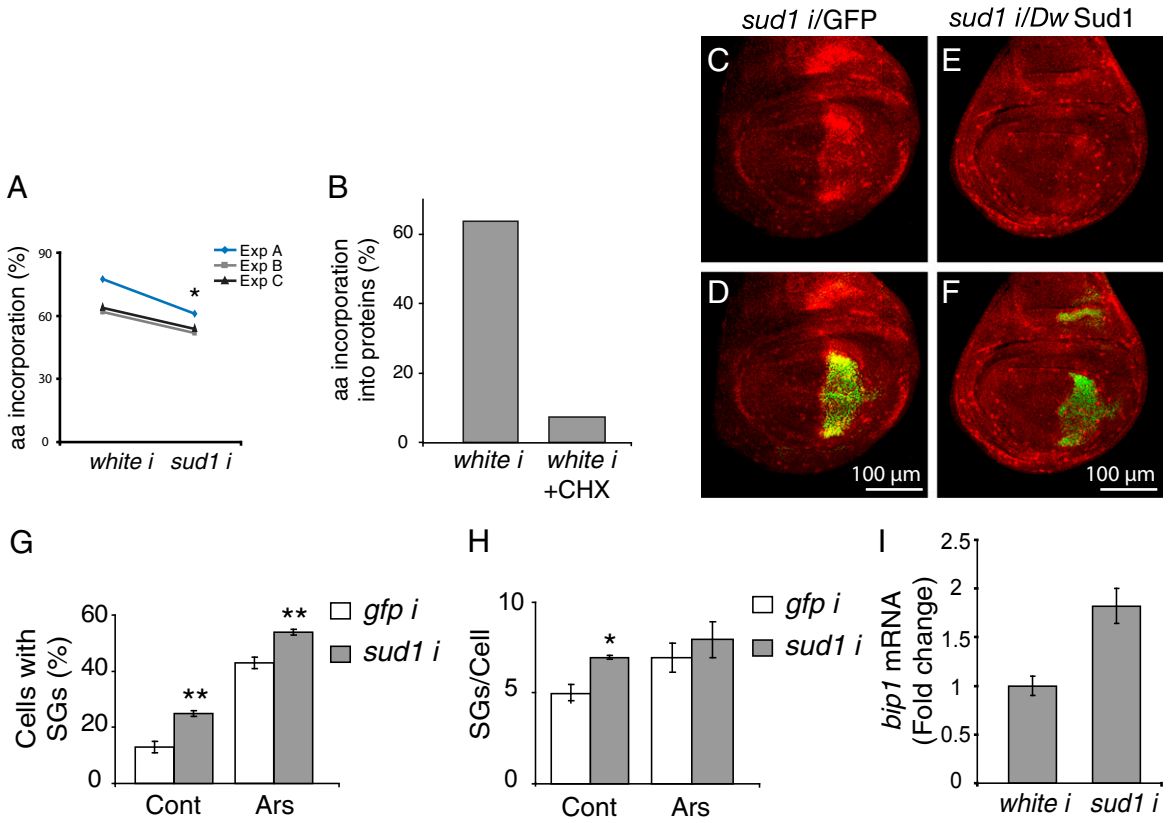

Fig. S4. Sud1 silencing inhibits protein synthesis, promotes stress granule formation, and triggers the unfolded protein response. (*A*) Sud1 silencing inhibits protein synthesis. Third-instar larvae wing imaginal discs were incubated with a mixture of [^{14}C]-labeled amino acids, and disc extracts were subjected to trichloroacetic acid (TCA) precipitation; the proportion of TCA-precipitated radioactivity in relation to total radioactivity incorporated into the discs in three independent experiments is shown ($n = 40$ discs). Data were analyzed with randomized blocks ANOVA. Paired measurements (including the two genotypes; $^{*}P < 0.05$). (B) Ex vivo incorporation of [^{14}C]-labeled amino acids into proteins of wing discs is strongly suppressed in a negative control experiment in which cycloheximide has been added to the incubation medium. (*C* and *D*) Wing discs accumulate P-eIF2a at the posterior compartment after expression of *sud1* RNAi. This accumulation is suppressed by concomitant expression of a *sud1 Drosophila willistoni* transgene (*E* and *F*), indicating that augmented phosphorylation of eIF2a is indeed due to Sud1 silencing. Green, anti-Engrailed staining. Quantification of the cells exhibiting SGs (*G*), as well as of the number of SGs per cell (*H*), was carried out automatically using the BUHO algorithm (*Materials and Methods*). Error bars represent SD. Two-way ANOVA with Bonferroni post hoc test ($^{*}P < 0.01$ and $^{**}P < 0.001$). (*I*) The Xbp-1 target *bip1* is induced after *actin*-Gal4 driven expression of *sud1* but not of *white* RNAi in first-instar larvae, as determined by qRT-PCR; error bars represent SD.

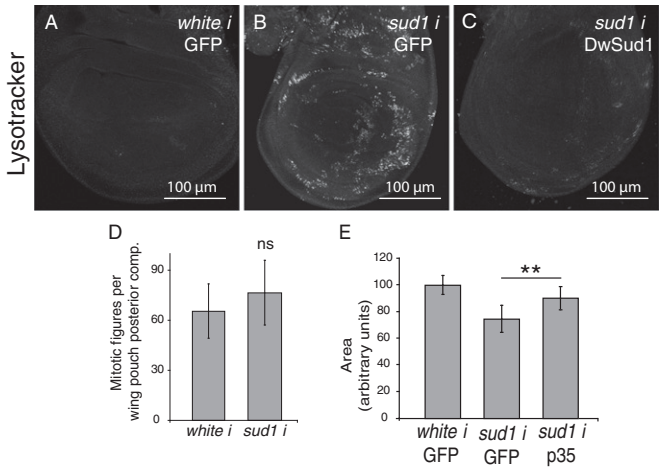

Fig. S5. After Sud1 silencing, autophagy and apoptosis are induced, but cell proliferation is unaffected. Lysotracker-positive staining in the posterior compartment of wing discs that express *sud1* RNAi (*B*) but not a control *white* RNAi (*A*) indicates that Sud1 silencing triggers autophagy. The Lysotracker-positive signal is suppressed after concomitant expression of a *Drosophila willistoni sud1* transgene (*C*). (*D*) *sud1* RNAi expression in the wing disc posterior compartment does not modify the number of cells that enter mitosis, as assessed by anti–phospho-Histone3 (PH3) immunofluorescence. The number of PH3-positive cells was analyzed in discs expressing *sud1* RNAi in comparison with control discs that express a *white* double stranded RNA. $n \geq 10$ imaginal discs. Error bars represent SD. ns, nonsignificant difference (Student *t* test). (*E*) Reduction of the area of the wing posterior compartment is partially suppressed by expression of the caspase inhibitor p35. $n \geq 30$ wings in three independent experiments. Error bars represent SD. One-way ANOVA with Tukey post hoc test (**$P < 0.01$).

Table S1. Loss of function screen for *Drosophila* dioxygenases required for wing normal growth

Gene	RNAi Line (VDRC number)	Intensity of growth phenotype	References
CG31543 (Fatiga)	KK103382	++	1
CG8421	KK101484	+	
CG44254	GD3402	+++	
CG31014	KK101152	–	
CG18749	GD15364	–	
CG9698	KK100678	–	
CG31022	GD2464	–	
CG9720	KK100523	–	
CG9726	KK101283	–	
CG31016	GD21280	–	
CG9728	KK102038	–	
CG18233	KK101594	–	
CG1546	KK107425	–	
CG32199	GD21601/ GD21600	–	
CG31524	KK100877	–	
CG32201	GD47008	–	
CG15864	KK105061	+	
CG18231	KK101201	–	
CG11828	KK101020	–	
CG18234	GD19187	–	
CG6199	GD45486/ GD45484	–	
CG7200	GD27913	–	
CG10133	GD18014/ KK108848	–	
CG2982	KK107819	+	
CG5640 (dUTX)	GD37664/ GD37663/ KK105986	+	2–4
CG9088 (LID)	KK103830/ GD42204	++	5, 6
CG33182 (dKdm4B)	GD46444	–	7
CG15835 (dKdm4A)	KK107868	+	8, 9
CG3654	GD21700	–	
CG11033 (dKdm2)	GD31402	–	10
CG33250	GD46450/ GD46452	–	
CG4036	GD26370	–	
CG6144	GD41847	–	
CG14130	GD31911	–	
CG14688	GD39840	–	
CG4335	KK105611	–	
CG10814	KK108425	–	
CG5321	GD22061	–	
CG14630	KK101204	+++	
CG33099	KK104229	–	
CG5346	KK101879	–	
CG33093	GD48795/ GD48796	–	

An RNAi-based screen was carried out to define which *Drosophila* dioxygenases are required for normal wing growth. Double-stranded RNAs (second column) against each of the predicted 2OG-dependent dioxygenases encoded in the *Drosophila* genome (first column) were expressed in transgenic lines under control of an *ms1096*-Gal4 driver, which induces expression exclusively at the disc dorsal compartment. Inhibition of growth of this compartment leads to development of wings that are curved upward. Depending on the intensity of the wing curvature, the phenotypes were classified as strong (+++), intermediate (++), or weak (+) (third column). Nine of the 42 presumptive dioxygenases scored as positives in the screen. The names of the genes that have been analyzed are quoted in parentheses, and the corresponding references are in the fourth column of the table.

1. Centanin L, Ratcliffe PJ, Wappner P (2005) Reversion of lethality and growth defects in Fatiga oxygen-sensor mutant flies by loss of hypoxia-inducible factor-alpha/Sima. *EMBO Rep* 6(11):1070–1075.
2. Tie F, Banerjee R, Conrad PA, Scacheri PC, Harte PJ (2012) Histone demethylase UTX and chromatin remodeler BRM bind directly to CBP and modulate acetylation of histone H3 lysine 27. *Mol Cell Biol* 32(12):2323–2334.
3. Herz HM, et al. (2010) The H3K27me3 demethylase dUTX is a suppressor of Notch- and Rb-dependent tumors in Drosophila. *Mol Cell Biol* 30(10):2485–2497.
4. Smith ER, et al. (2008) Drosophila UTX is a histone H3 Lys27 demethylase that colocalizes with the elongating form of RNA polymerase II. *Mol Cell Biol* 28(3):1041–1046.
5. Secombe J, Li L, Carlos L, Eisenman RN (2007) The Trithorax group protein Lid is a trimethyl histone H3K4 demethylase required for dMyc-induced cell growth. *Genes Dev* 21(5): 537–551.
6. Lee N, et al. (2007) The trithorax-group protein Lid is a histone H3 trimethyl-Lys4 demethylase. *Nat Struct Mol Biol* 14(4):341–343.
7. Palomera-Sanchez Z, Bucio-Mendez A, Valadez-Graham V, Reynaud E, Zurita M (2010) Drosophila p53 is required to increase the levels of the dKDM4B demethylase after UV-induced DNA damage to demethylate histone H3 lysine 9. *J Biol Chem* 285(41):31370–31379.
8. Lin CH, et al. (2008) Heterochromatin protein 1a stimulates histone H3 lysine 36 demethylation by the Drosophila KDM4A demethylase. *Mol Cell* 32(5):696–706.
9. Lorbeck MT, et al. (2010) The histone demethylase Dmel\Kdm4A controls genes required for life span and male-specific sex determination in Drosophila. *Gene* 450(1-2):8–17.
10. Lagarou A, et al. (2008) dKDM2 couples histone H2A ubiquitylation to histone H3 demethylation during Polycomb group silencing. *Genes Dev* 22(20):2799–2810.

Table S2. Reduction of function of the TOR pathway partially suppresses growth inhibition provoked by Sudestada1 silencing

Allele	Nuclear area (% of control)		Nuclear area reduction (%)(*white* RNAi − *sud1* RNAi)
	white RNAi	*sud1* RNAi	
yw	100 ± 18.8	61 ± 10.2	39
tor^{2L1}	97.2 ± 14.5	86.4 ± 13.6**	11.2
tsc^{Q87X}	98.9 ± 12.5	61.3 ± 20.4	38
$S6K^{L1}$	94.9 ± 17.3	78.6 ± 17.3**	17.2
$rheb^{P\Delta1}$	93.9 ± 11.3	66.7 ± 16	29
$rheb^{P\Delta2}$	94 ± 12.4	68.2 ± 16.8	27.4
4E-BP ($thor^2$)	91 ± 10.8	48.3 ± 6.9*	46.9

sud1 RNAi was expressed under control of a *ppl*-Gal4 driver, and the area of nuclei of fat body cells was measured in third-instar larvae that were heterozygous for the indicated loss of function alleles of genes of the TOR pathway. Note that growth inhibition provoked by *sud1* RNAi expression is alleviated in TOR^{2L1} and $S6K^{L1}$ heterozygous larvae, and conversely, it is enhanced in 4E-BP($thor^2$) heterozygous individuals. $n \geq 300$ nuclei in three independent experiments. Error bars represent SD. Two-way ANOVA with Tukey post hoc test (*$P < 0.05$ and **$P < 0.001$). In the case of 4E-BP, the data were transformed to $\log_{10}$.